Pergamon

Int. J. Solids Structures Vol. 34, No. 25, pp. 3273–3289, 1997

0020-7683/97 $17.00 + .00

PII: S0070-7683(96)00213-2

CYCLIC EFFECTS IN SHAPE-MEMORY ALLOYS: A ONE-DIMENSIONAL CONTINUUM MODEL

ROHAN ABEYARATNE and SANG-JOO KIM
Department of Mechanical Engineering, Massachusetts Institute of Technology, Cambridge, MA 02139, U.S.A.

(*Received* 23 *August* 1995; *in revised form* 25 *September* 1996)

Abstract—We generalize the thermoelastic constitutive model of Abeyaratne and Knowles (1993, *J. Mech. Phys. Solids* **41**, 541–571), and Abeyaratne *et al.* (1994, *Int. J. Solids Structures* **31**, 2229–2249) so as to qualitatively model a variety of phenomena exhibited by shape-memory alloys in cyclic loading. The internal variable that is added to the model is meant to capture the idea that defects are precipitated during transformation and that these defects tend to make the nucleation of martensite easier. © 1997 Elsevier Science Ltd.

1. INTRODUCTION

Shape-memory alloys can respond to cyclic loading in interesting ways. e.g. under tensile loading, the stress–elongation hysteresis loop that is characteristic of the pseudoelastic behaviour of these materials drifts downwards with increasing load cycles and eventually settles onto a limiting loop (e.g. Miyazaki *et al.*, 1986a; Kawaguchi *et al.*, 1991; Lin *et al.*, 1994; Tobushi *et al.*, 1991). On the other hand, when the loading involves both tension and compression, Lieberman *et al.* (1975), observed in Au–Cd that the response starts out involving two separate hysteresis loops that are joined to each other by a reversible branch, but that after a sufficiently large number of cycles, these two loops coalesce into one. A hysteresis loop with a staircase-like structure has been observed by Kyriakides and Shaw (1995) in cyclic experiments in which the amplitude of the applied elongation was increased from one cycle to the next. Perhaps the most striking consequence of cyclic loading is the so-called two-way shape-memory effect: when a virgin specimen of austenite is subjected to thermal cycling, it exhibits the usual (small) length change associated with thermal expansion and contraction. However, if such a specimen is first subjected to mechanical cycling in tension, subsequent (stress-free) thermal cycling exhibits significant length changes, an extension associated with cooling and a contraction associated with heating [see e.g. Perkins and Sponholz (1984)].

A number of constitutive models for describing the response of shape-memory alloys have been proposed (e.g. Abeyaratne and Knowles, 1993; Abeyaratne *et al.*, 1994; Brinson and Lammering, 1993; Falk, 1980; Graesser and Cozzarelli, 1994; Müller and Wilmansky, 1981; Müller and Xu, 1991; Ortin, 1992; Raniecki *et al.*, 1992, etc). None of these models is able to capture all of the aforementioned phenomena associated with cyclic loading.

The principal microstructural reasons for these characteristics is the generation of defects [see Melton and Mercier (1979); Perkins and Sponholz (1984); Miyazaki *et al.* (1986a, b)]. During thermomechanical cycling, austenite–martensite phase boundaries travel back and forth through the specimen. Since the crystallographic lattices do not match perfectly across such an interface, microstructural defects such as dislocations are associated with the propagating front and are left behind in the transformed material.

A continuum model which does take this observation into account and which was proposed specifically in order to describe the cyclic behavior of shape-memory alloys, is the one of Tanaka *et al.* (1992; 1993). They took the point of view that the defects generated by the moving austenite–martensite interface lead to the accumulation of microscopic residual stress and strain fields in the alloy. Accordingly, they introduced three internal

variables into their stress–strain relation, two of which describe the microscopic residual stress and strain, and the third characterizing the volume fraction of the residual martensite.

In this paper we present a different model, which we construct by slightly generalizing the aforementioned model of Abeyaratne and Knowles (1993) and Abeyaratne *et al.* (1994). The key difference between our model and that of Tanaka *et al.* (1992; 1993) is that we take an energetic point of view. As mentioned above, the defects generated in a particular loading cycle "stabilizes martensite", i.e. the transformation to martensite becomes easier in each subsequent loading cycle, while the transformation out of martensite progressively becomes more difficult. From an energetic point of view, one can model this in one of two ways: either, by letting the height between the martensitic and austenitic energy wells depend on the defect density in such a way that martensite becomes intrinsically more stable (Kim and Abeyaratne, 1995); or, by allowing the energy barriers between austenite and martensite to be effectively changed by the defects in such a way that the nucleation and kinetics of the transformation process favors martensite. Here, we adopt this second point of view. We introduce an internal variable into the model of Abeyaratne *et al.* (1994) which affects the nucleation level of the thermodynamic driving force and the kinetics, but not the stress–strain–temperature relation. An attractive feature of the present model is that we are able to simulate both mechanical and thermal cycling, and in particular, to simulate all of the phenomena described in the first paragraph of this section.

2. CONSTITUTIVE MODEL

In this section we will briefly review the constitutive model studied by Abeyaratne *et al.* (1994). This model for thermoelastic phase transformations was designed to be as simple as possible, while at the same time explicitly building upon the fact that the essential underlying mechanism is the transition of the material from one energy well to another. The model incorporates the multiple-well structure of the free energy function and includes explicitly a kinetic rule that characterizes the rate of transition from one energy well to another, as well as a nucleation rule signalling the commencement of the transformation process.

2.1. *Helmholtz free-energy*

The Helmholtz free-energy function $\psi(\gamma, \theta)$, where γ is strain and θ is temperature, constructed in Abeyaratne *et al.* (1994) was designed to describe a material which can exist in an austenitic phase A and a martensitic phase with two variants M^+ and M^-. At high temperatures, $\psi(\cdot, \theta)$ has a single minimum corresponding to austenite; for a range of intermediate temperatures it has three local minima corresponding to austenite and the two martensitic variants; and at low temperatures it has two local minima associated with the martensitic variants. The two martensitic energy wells (local minima) were arranged to have the same height at all temperatures since they corresponded to variants of a single phase. At the transformation temperature θ_T all three energy wells have the same height; the austenitic energy well is lower than the martensitic wells for $\theta > \theta_T$, while the martensitic wells are lower for $\theta < \theta_T$. Specifically:

$$\rho\psi = \begin{cases} (\mu/2)\gamma^2 - \mu\alpha\gamma(\theta-\theta_T) + \rho c\theta(1-\log(\theta/\theta_T)) & \text{for } A, \\ (\mu/2)(\gamma-\gamma_T)^2 - \mu\alpha(\gamma-\gamma_T)(\theta-\theta_T) + \rho c\theta(1-\log(\theta/\theta_T)) & \\ -\rho\lambda_T(1-\theta/\theta_T) & \text{for } M^+, \\ (\mu/2)(\gamma+\gamma_T)^2 - \mu\alpha(\gamma+\gamma_T)(\theta-\theta_T) + \rho c\theta(1-\log(\theta/\theta_T)) & \\ -\rho\lambda_T(1-\theta/\theta_T) & \text{for } M^-. \end{cases} \tag{1}$$

We refer the reader to Abeyaratne *et al.* (1994) for a more complete description, including a characterization of the specific regions of the γ, θ-plane on which each of these three expressions for ψ hold. Two subsequent figures in the present paper make reference to

temperature levels θ_M and θ_m; the former is the highest temperature that we consider, whereas the latter is the temperature below which austenite does not exist.

The material constants involved in eqn (1) are the elastic modulus μ, the specific heat at constant strain c and the coefficient of thermal expansion α, each of which has been assumed for simplicity to have the same value for all three phases; the mass density ρ in the reference state; the transformation temperature θ_T; the latent heat λ_T at the temperature θ_T; and the transformation strain $\gamma_T > 0$.

Terminology: for simplicity, we sometimes speak of "three phases" rather than "one phase and two variants"; similarly we shall use the term "phase boundary" generically to refer to both an interface between two phases and to an interface between two variants.

The various other thermo-mechanical characteristics of the material can be derived from eqn (1). In particular, the relation between stress, strain and temperature is given by

$$\sigma = \hat{\sigma}(\gamma, \theta) = \rho\psi_\gamma(\gamma, \theta) = \begin{cases} \mu\gamma - \mu\alpha(\theta - \theta_T) & \text{for } A, \\ \mu(\gamma - \gamma_T) - \mu\alpha(\theta - \theta_T) & \text{for } M^+, \\ \mu(\gamma + \gamma_T) - \mu\alpha(\theta - \theta_T) & \text{for } M^-. \end{cases} \tag{2}$$

Graphs of $\hat{\sigma}(\gamma, \theta)$ versus γ at two fixed temperatures are shown in Fig. 1: Fig. 1(a) corresponds to a fixed value of temperature at which all three phases exist, and the stress–strain curve shows three rising branches corresponding to A, M^+ and M^-; Fig. 1(b) is

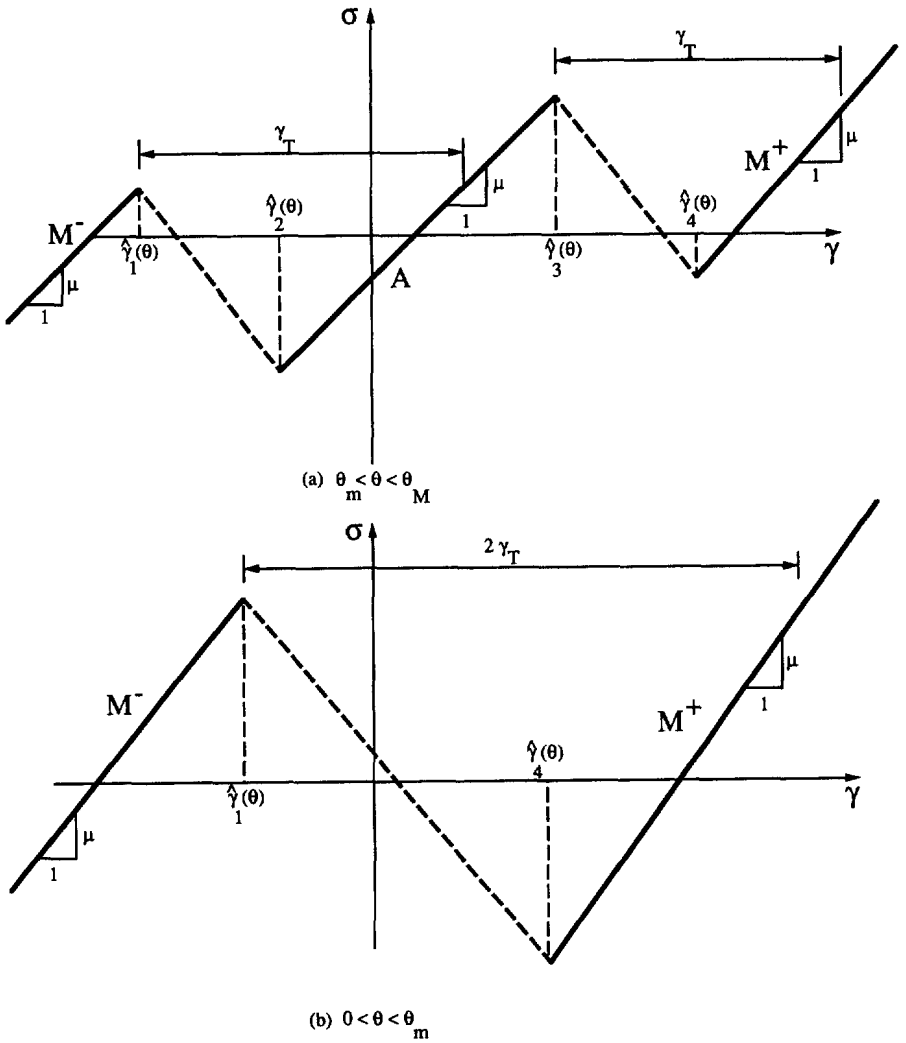

Fig. 1. Stress–strain curves at constant temperature θ.

associated with a lower value of temperature, one at which only martensite exists, as indicated by the two rising branches of the stress–strain curve.

Next, consider the relative stability of these three phases. Suppose that at some given stress and temperature, a particle has a choice of which phase it can be in. From among the possibilities, one speaks of the phase with the smallest value of Gibbs free energy $g = \rho\psi - \sigma\gamma$ as the stable phase. An explicit expression for g for each phase can be calculated using eqns (1) and (2) leading to

$$\begin{aligned}
g &= -\frac{1}{2\mu}[\sigma+\mu\alpha(\theta-\theta_T)]^2+\rho c\theta\left[1-\log\left(\frac{\theta}{\theta_T}\right)\right] && \text{for } A,\\
g &= -\frac{1}{2\mu}[\sigma+\mu\alpha(\theta-\theta_T)]^2+\rho c\theta\left[1-\log\left(\frac{\theta}{\theta_T}\right)\right]-\rho\lambda_T\left(1-\frac{\theta}{\theta_T}\right)-\sigma\gamma_T && \text{for } M^+,\\
g &= -\frac{1}{2\mu}[\sigma+\mu\alpha(\theta-\theta_T)]^2+\rho c\theta\left[1-\log\left(\frac{\theta}{\theta_T}\right)\right]-\rho\lambda_T\left(1-\frac{\theta}{\theta_T}\right)+\sigma\gamma_T && \text{for } M^-.
\end{aligned} \tag{3}$$

By comparing these values of g with each other, it follows that for $\theta > \theta_T$, austenite is stable if

$$\sigma_0(\theta) > \sigma > -\sigma_0(\theta), \tag{4}$$

M^+ martensite is stable if

$$\sigma > \sigma_0(\theta), \tag{5}$$

and M^- martensite is stable if

$$\sigma < -\sigma_0(\theta), \tag{6}$$

where we have set

$$\sigma_0(\theta) = \frac{\rho\lambda_T}{\gamma_T}\left(\frac{\theta}{\theta_T}-1\right). \tag{7}$$

On the other hand, for $\theta < \theta_T$, one finds that M^+ martensite is stable if σ is positive whereas M^- is stable if $\sigma < 0$. Figure 2 displays the domains of the (θ, σ)-plane characterized by eqns (4)–(6) on which the different phases are stable. The boundaries between these regions, the so-called "Maxwell-lines", are given by $\sigma = 0$ and $\sigma = \pm\sigma_0(\theta)$. Observe from the figure that at temperatures below the transformation temperature θ_T, M^- is stable under compressive stress while M^+ is stable under tensile stress. Observe also that at a fixed stress, austenite becomes stable if the temperature is sufficiently high.

2.2. *Nucleation criterion*

Abeyaratne *et al.* (1994) supposed that nucleation is based on a critical value of driving force. More specifically, they assumed that a new phase ("product phase") is nucleated within a single phase state ("parent phase") when the resulting decrease in Gibbs free-energy reaches a critical value:

$$g_{\text{parent}} - g_{\text{product}} = f_{\text{cr}}. \tag{8}$$

For simplicity of the present discussion, we shall take the nucleation level f_{cr} to be the same for transitions from any parent phase (A, M^+ or M^-) to any other product phase (A, M^+ or M^-). It will sometimes be more convenient in what follows to work with the stress-level

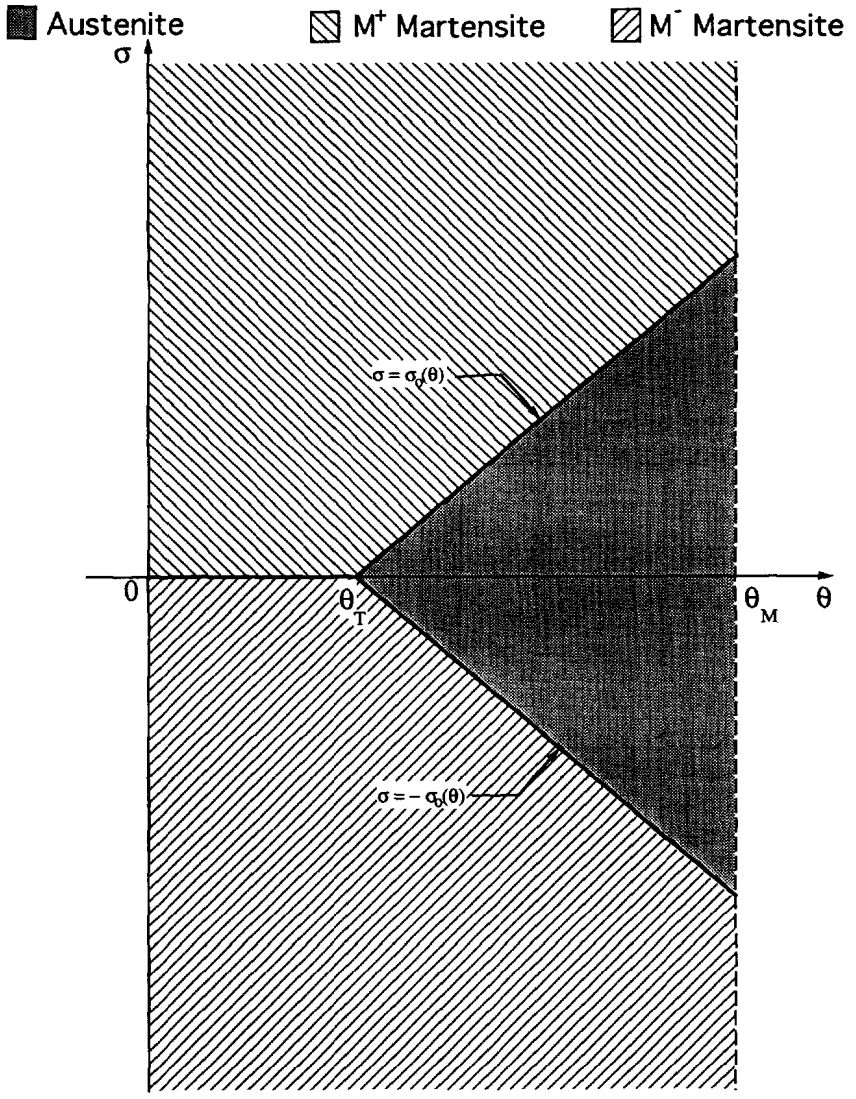

Fig. 2. The stable phases.

σ_{cr} defined by

$$f_{cr} = \sigma_{cr}\gamma_T \geqslant 0; \tag{9}$$

the inequality in eqn (9) follows the thermodynamic requirement that g_{parent} cannot be less than $g_{product}$.

For each transformation, the value of the Gibbs free-energies g_{parent} and $g_{product}$ of each phase can be obtained from eqn (3). This, together with eqns (8) and (9), yields the following explicit nucleation conditions:

$$\left.\begin{aligned}
&\sigma = \sigma_{cr} + \sigma_0(\theta) && \text{for } A \to M^+,\\
&\sigma = -\sigma_{cr} + \sigma_0(\theta) && \text{for } M^+ \to A,\\
&\sigma = -\sigma_{cr} - \sigma_0(\theta) && \text{for } A \to M^-,\\
&\sigma = \sigma_{cr} - \sigma_0(\theta) && \text{for } M^- \to A,\\
&\sigma = -\sigma_{cr}/2 && \text{for } M^+ \to M^-,\\
&\sigma = \sigma_{cr}/2 && \text{for } M^- \to M^+.
\end{aligned}\right\} \tag{10}$$

The nucleation conditions, eqn (10), can be described by three pairs of straight lines in the

(θ, σ)-plane. Each pair is parallel to, and lies on either side of, the corresponding stability boundary shown in Fig. 2. If $f_{cr} = 0$, or equivalently $\sigma_{cr} = 0$, the nucleation lines coincide with the stability boundaries.

If a specimen of austenite is cooled under stress-free conditions, martensite is nucleated at the so-called "martensite-start" temperature denoted by M_s. Similarly the "austenite-start" temperature A_s denotes the temperature at which austenite is nucleated in stress-free martensite when it is heated. These temperatures can be found by setting $\sigma = 0$, $\theta = M_s$ in eqn (10a) and $\sigma = 0$, $\theta = A_s$ in eqn (10b)

$$M_s = \theta_T\left[1 - \frac{\sigma_{cr}\gamma_T}{\rho\lambda_T}\right], \quad A_s = \theta_T\left[1 + \frac{\sigma_{cr}\gamma_T}{\rho\lambda_T}\right]. \tag{11}$$

It is worth noting that upon using eqns (7) and (11), the first four nucleation conditions in eqn (10) can be written in the alternative form

$$\left.\begin{aligned} \theta &= M_s \pm \frac{\gamma_T\theta_T}{\rho\lambda_T}\sigma \quad \text{for } A \to M^{\pm}, \\ \theta &= A_s \pm \frac{\gamma_T\theta_T}{\rho\lambda_T}\sigma \quad \text{for } M^{\pm} \to A. \end{aligned}\right\}$$

2.3. *Kinetic relation*

Finally, consider the kinetic relation which characterizes the rate at which the transformation progresses once it has nucleated. Consider a bar composed of the material at hand, which has a phase boundary at some location $x = s(t)$. In general, the kinetic law is a relation between the propagation velocity $\dot{s}$ of the phase boundary, the driving force f on that phase boundary and the local temperature θ: $\dot{s} = \phi(f, \theta)$. In the present paper we explore the special case of such a relation

$$\dot{s} = \begin{cases} \leqslant 0 & \text{for } f = -f_{cr}, \\ 0 & \text{for } -f_{cr} < f < f_{cr}, \\ \geqslant 0 & \text{for } f = f_{cr}. \end{cases} \tag{12}$$

Here the material constant $f_{cr} = \sigma_{cr}\gamma_T$ is the nucleation level of driving force introduced earlier. According to this kinetic model, a phase boundary cannot propagate if the driving force lies in the range $-f_{cr} < f < f_{cr}$; when the phase boundary propagates to the right one has $f = f_{cr}$ (and $f = -f_{cr}$ when the phase boundary propagates to the left). Such a "friction-like" kinetic relation can be associated with a certain notion of maximum dissipation and is reminiscent of elastic–perfectly plastic behavior.

In order to utilize the above kinetic relation, one must calculate explicit expressions for the driving force f on an interface separating two phases. Since, in the present setting, the driving force equals the difference in the Gibbs free-energy across that interface, one can calculate f on all possible interfaces using eqn (3), leading to

$$\left.\begin{aligned} f &= [\sigma - \sigma_0(\theta)]\gamma_T && \text{for a } M^+/A \text{ interface}, \\ f &= -[\sigma - \sigma_0(\theta)]\gamma_T && \text{for an } A/M^+ \text{ interface}, \\ f &= [\sigma + \sigma_0(\theta)]\gamma_T && \text{for an } A/M^- \text{ interface}, \\ f &= -[\sigma + \sigma_0(\theta)]\gamma_T && \text{for a } M^-/A \text{ interface}, \\ f &= 2\sigma\gamma_T && \text{for a } M^+/M^- \text{ interface}, \\ f &= -2\sigma\gamma_T && \text{for a } M^-/M^+ \text{ interface}, \end{aligned}\right\} \tag{13}$$

where by an "I/J-interface" we mean a phase boundary which has phase-I on its left and

phase-J on its right, and the driving force is defined as the value of g on the right-hand side of the interface minus its value on the left: $f = g_J - g_I$. Note that if an I/J phase boundary propagates to the right, it transforms material from phase J to phase I, so that J is then the parent phase while I is the product phase. The converse is true if it propagates to the left.

3. EFFECT OF DEFECTS ON CONSTITUTIVE MODEL

We now generalize the constitutive model described in the preceding section so as to be able to describe cyclic phenomena. Of the three ingredients in that model, we shall modify the description of nucleation and kinetics, but leave eqn (1), the energy wells of the Helmholtz free-energy function, unchanged.

In the model of Abeyaratne *et al.* (1994) the nucleation level of driving force f_{cr} was assumed to be constant. However, due to the lack of perfect geometric compatibility across an austenite–martensite interface, a propagating phase boundary that transforms austenite into martensite often generates lattice defects such as dislocations. The defects that are thus generated remain dispersed throughout the transformed region and play a critical role in making subsequent transformations to martensite easier. The reverse transformation from martensite to austenite does not remove the defects generated by the forward transformation nor does it generate any additional defects [see Miyazaki *et al.* (1986a)].

It is natural to suppose that the defects that are left behind act as local stress concentrators which favor the formation of martensite. Consequently, the critical value of driving force required for nucleating and propagating the various transformations would be affected by the defect density ($\approx$ the number of loading cycles).

Let x denote the Lagrangian coordinate of a particle in the reference configuration. Let $\overset{+}{n}(x,t)$ and $\overset{-}{n}(x,t)$ be the number of times that this particle has undergone the respective transitions $A \to M^+$ and $A \to M^-$ in its entire past history up to time t. Then, the driving force $g_{\text{parent}} - g_{\text{product}}$ required for transformation in the next loading cycle will be related to its original value f_{cr} in the following way: since the transformation from austenite to martensite becomes easier with cycling, the nucleation level of driving force for the $A \to M^+$ transition must decrease monotonically as $\overset{+}{n}$ increases and similarly that for the $A \to M^-$ transition must decrease as $\overset{-}{n}$ increases; likewise, since the reverse transition from martensite to austenite becomes more difficult, the nucleation level of driving force for the $M^+ \to A$ and $M^- \to A$ transitions must be increased. Finally, since the defects generated by the $\overset{+}{n}$ prior transformations from $A \to M^+$ lead to a favoring of M^+ martensite, while the $\overset{-}{n}$ prior transformations from $A \to M^-$ favor M^- martensite, we would expect that the nucleation level of the driving force for the $M^+ \to M^-$ transition is reduced if $\overset{-}{n} > \overset{+}{n}$ and is increased if $\overset{-}{n} < \overset{+}{n}$. A similar statement for the reverse $M^- \to M^+$ transition can be made.

In order to quantify this, let $\Sigma(n)$ be any monotonically increasing function with $\Sigma(0) = 0$ and $\Sigma(\infty)$ finite. Then, one set of nucleation criteria which is consistent with the above qualitative description is the following: a transformation from a parent phase (A, M^+, M^-) to a product phase (A, M^+, M^-) occurs when

$$g_{\text{parent}} - g_{\text{product}} = F_{cr} = \begin{cases} f_{cr} - \gamma_T \Sigma(\overset{+}{n}) & \text{for } A \to M^+, \\ f_{cr} - \gamma_T \Sigma(\overset{-}{n}) & \text{for } A \to M^-, \\ f_{cr} + \gamma_T \Sigma(\overset{+}{n}) & \text{for } M^+ \to A, \\ f_{cr} + \gamma_T \Sigma(\overset{-}{n}) & \text{for } M^- \to A, \\ f_{cr} + \gamma_T [\Sigma(\overset{-}{n}) - \Sigma(\overset{+}{n})] & \text{for } M^- \to M^+, \\ f_{cr} + \gamma_T [\Sigma(\overset{+}{n}) - \Sigma(\overset{-}{n})] & \text{for } M^+ \to M^-; \end{cases} \tag{14}$$

here $f_{cr} > 0$ is constant, as before. This is our generalization of the nucleation criterion, eqn (8). For thermodynamically admissible nucleation, one must have $F_{cr} \geqslant 0$; it follows,

recalling the properties of $\Sigma(n)$ described above, that

$$\sigma_{cr} \geqslant \Sigma(\infty) \tag{15}$$

where $\sigma_{cr} = f_{cr}/\gamma_T$.

Proceeding as before, for each transformation, the values of the Gibbs free-energies g_{parent} and $g_{product}$ of each phase can be taken from eqn (3). Using this information in the nucleation criteria, eqn (14), one obtains

$$\left.\begin{aligned}
&\sigma = \sigma_{cr} + \sigma_0(\theta) - \Sigma(\overset{+}{n}) && \text{for } A \to M^+,\\
&\sigma = -\sigma_{cr} + \sigma_0(\theta) - \Sigma(\overset{+}{n}) && \text{for } M^+ \to A,\\
&\sigma = -\sigma_{cr} - \sigma_0(\theta) + \Sigma(\overset{-}{n}) && \text{for } A \to M^-,\\
&\sigma = \sigma_{cr} - \sigma_0(\theta) + \Sigma(\overset{-}{n}) && \text{for } M^- \to A,\\
&\sigma = -\frac{\sigma_{cr}}{2} + \frac{\Sigma(\overset{-}{n}) - \Sigma(\overset{+}{n})}{2} && \text{for } M^+ \to M^-,\\
&\sigma = \frac{\sigma_{cr}}{2} + \frac{\Sigma(\overset{-}{n}) - \Sigma(\overset{+}{n})}{2} && \text{for } M^- \to M^+,
\end{aligned}\right\} \tag{16}$$

where we have also used eqn (9). Equation (16) is the generalized version of eqn (10).

For fixed values of the number of load cycles $\overset{+}{n}$ and $\overset{-}{n}$, the nucleation criteria, eqn (16) may be described in the θ, σ-plane by three pairs of straight lines (Fig. 3). A thermomechanical loading process $(\theta(t), \sigma(t))$, $t_0 \leqslant t \leqslant t_1$, corresponds to an oriented curve in this plane and the material undergoes a particular transformation whenever this curve crosses the associated nucleation line in the direction of the arrows in Fig. 3. When the material is subjected to a cyclic loading history, $\overset{+}{n}$ and/or $\overset{-}{n}$ increase, and so the nucleation lines drift in the θ, σ-plane; since $\Sigma(n)$ is a monotonically increasing function, they in fact translate in a definite direction as the number of load cycles increase. Figure 4 shows these nucleation lines for three different values of $(\overset{+}{n}, \overset{-}{n})$. For example, it follows from eqn (16a, b) that when $\overset{+}{n}$ increases, the nucleation lines associated with the $A \to M^+$ transitions translate rigidly to the right; thus, the nucleation stress levels at a fixed temperature for both the $A \to M^+$ and $M^+ \to A$ transformations are decreased (Fig. 4); on the other hand, it is seen that the nucleation temperature levels at fixed stress are increased.

Next, consider the effect of the defects on the kinetic relation which governs the propagation of a phase boundary. Based on the observations above, the natural generalization of the kinetic law, eqn (12) of the original model is

$$\dot{s} = \begin{cases} \leqslant 0 & \text{for } f = -F_{cr},\\ 0 & \text{for } -F_{cr} < f < F_{cr},\\ \geqslant 0 & \text{for } f = F_{cr}, \end{cases} \tag{17}$$

where we have simply replaced f_{cr} in eqn (12) by the current nucleation level of driving force, F_{cr}; eqn (14).

Finally, we turn to the constitutive function $\Sigma(n)$. We emphasize at the outset that the analysis in this paper requires only that $\Sigma(0) = 0$, that $\Sigma(\cdot)$ be monotonically increasing and that $\Sigma(\infty)$ be finite. The specific form discussed below is presented solely for illustrative purposes and to make connection with experiments. Perkins and Sponholz (1984), Miyazaki *et al.* (1986a), Kyriakides and Shaw (1995), and others have carried out tensile (i.e. $A \to M^+$) cyclic loading experiments on shape-memory alloys. They found that the stress–elongation hysteresis loop drifts downwards with cycling, so that the stress levels associated with both the forward and reverse transformation decrease correspondingly. The amount

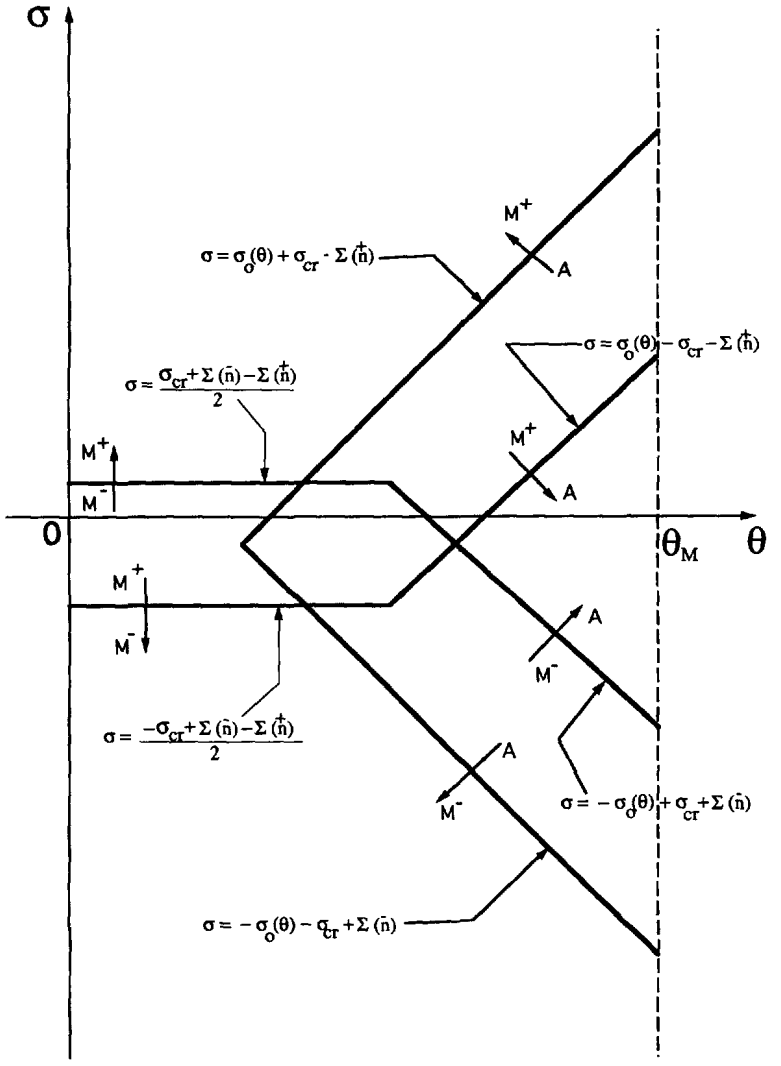

Fig. 3. Nucleation criteria.

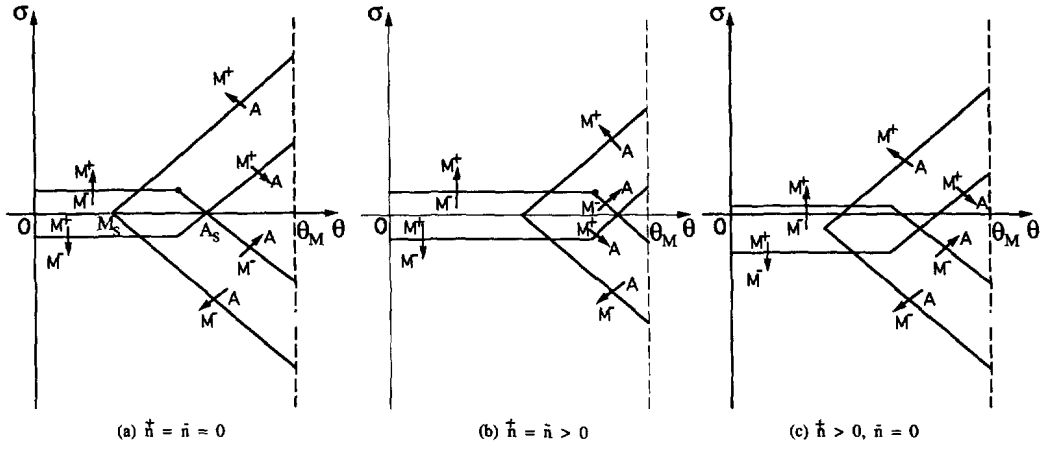

Fig. 4. Nucleation criteria—three cases.

of this decrement was found to decrease exponentially with the number of cycles and the transformation-stress levels eventually converge to certain limiting values. Since, according to eqn (16a, b) the decrement in stress level due to cycling between A and M^+ is $\Sigma(\overset{+}{n})$, this suggests that we take

$$\Sigma(n) = \Sigma_{\max}\left[1-\exp\left(-\frac{n}{n_0}\right)\right] \tag{18}$$

where the material constants $\Sigma_{\max}$ and n_0 are both positive, and $\Sigma_{\max} \leqslant \sigma_{cr}$ by eqn (15).

A constitutive function of the form (18) was previously considered by Tanaka *et al.* (1992; 1993) in their studies of cyclic loading, but they introduced such a term into the stress–strain relation (and therefore implicitly into the free-energy). Note that the term Σ does not enter our stress–strain–temperature relation, eqn (2). The way in which we introduce Σ allows us to simulate, among other things, the two-way shape memory effect.

4. RESULTS AND DISCUSSION

We now use the constitutive model described in Section 3 to calculate the uniaxial response of a bar subjected to various cyclic mechanical and thermal loadings.

Since we will only consider a uniform bar here, the stress field is necessarily spatially uniform. Thus, there is no preferred site for nucleation. If the bar had a uniformly tapered cross section with its left-hand end having the smallest area, nucleation would necessarily occur as follows: suppose that the bar consists entirely of a certain phase. Then, if a higher-strain phase nucleates, it would do so at the left end of the bar, whereas if a lower-strain phase nucleates this would occur at the right end. Thus, for example if the bar consists entirely of M^+, then austenite would nucleate at the right end, whereas if it consisted wholly of M^-, austenite would nucleate at the left end. In the uniform bar that we consider here, we shall (arbitrarily) take the nucleation sites to be given by this same rule.

(i) Consider an austenitic bar of length L which has never undergone a previous phase transformation; thus initially, $\overset{+}{n} = \overset{-}{n} = 0$. The bar is held at a fixed temperature $\theta > A_s$ [Fig. 4(a)] and is subjected to a prescribed cyclic extension $\delta(t)$. According to our model, the stress–elongation response during the nth-loading cycle is as follows: when the bar consists entirely of austenite, eqn (2a) gives

$$\sigma = \mu\delta/L - \mu\alpha(\theta-\theta_T); \tag{19}$$

by eqns (16a) and (17), the transformation from $A \to M^+$ occurs at the constant stress

$$\sigma = \sigma_{cr} + \sigma_0(\theta) - \Sigma(n); \tag{20}$$

when the bar consists entirely of martensite, eqn (2b) gives

$$\sigma = \mu(\delta/L - \gamma_T) - \mu\alpha(\theta-\theta_T); \tag{21}$$

and, according to eqns (16a) and (17), the reverse transformation from $M^+ \to A$ occurs at

$$\sigma = -\sigma_{cr} + \sigma_0(\theta) - \Sigma(n). \tag{22}$$

The term $\Sigma(n)$ increases monotonically from $\Sigma(0) = 0$ to $\Sigma(\infty)$ as the number of cycles n increases. Equations (20) and (22) describe the upper and lower plateaus of the hysteresis

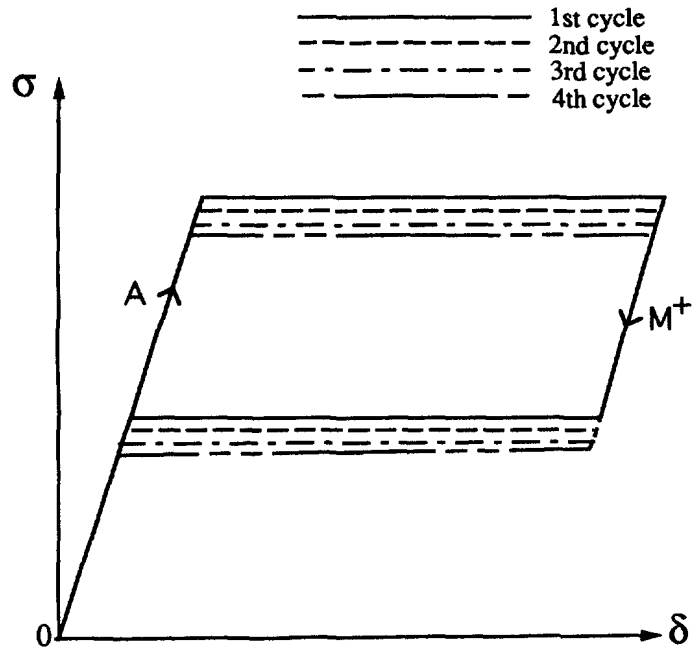

(a) Tensile cyclic loading: hysteresis loop drifts downwards.

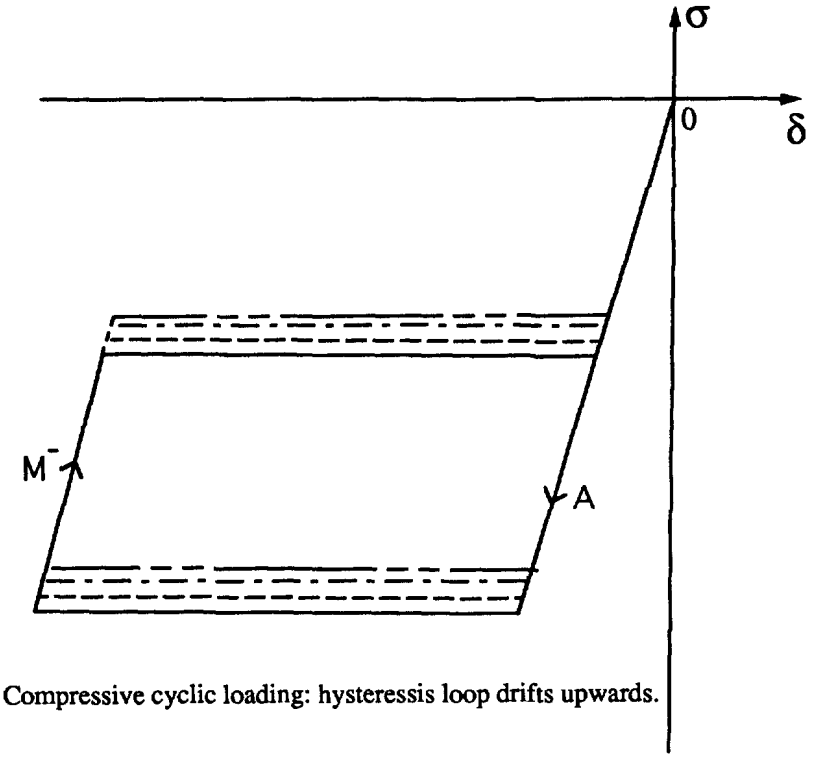

(b) Compressive cyclic loading: hysteressis loop drifts upwards.

Fig. 5. Stress–elongation hysteresis loops.

loop shown in Fig. 5(a). They drift downwards as n increases (in such a way that the height of the hysteresis loop does not change). The extent of this shift in each cycle gets smaller with increasing n. Figure 5(a) shows the stress–elongation hysteresis loops for the first four cycles of such a loading program. A response similar to this has been observed in experiments, e.g. Miyazaki *et al.* (1986a), Kawaguchi *et al.* (1991), Lin *et al.* (1994), Tobushi *et al.* (1991), and Kyriakides and Shaw (1995).

It should be noted that under certain conditions the lower plateau of this hysteresis loop may reach the horizontal axis after a certain number of cycles. If this happens,

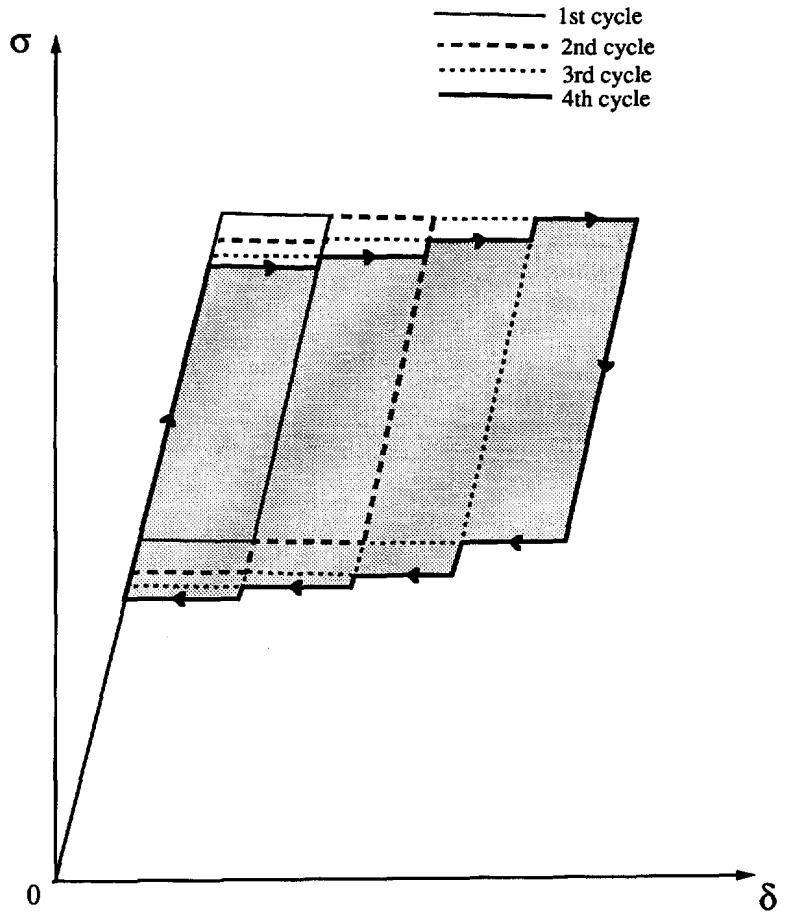

Fig. 6. Cyclic loading with loading amplitude increasing from one cycle to the next.

subsequent load cycles simply involve the deformation of pure martensite. From eqns (7) and (22), it is seen that this will happen only if the test temperature θ is less than $\theta_T[1+\gamma_T(\sigma_{cr}+\Sigma(\infty))/(\rho\lambda_T)]$. In this case, the number of cycles N after which austenite is not recovered upon unloading is given by the root of the equation $\theta = \theta_T[1+\gamma_T(\sigma_{cr}+\Sigma(N))/(\rho\lambda_T)]$. If θ exceeds this value, the hysteresis loop retains the general characteristics shown in Fig. 5(a) for all cycles and eventually converges to the loop described by eqns (19)–(22) with $\Sigma(n)$ replaced by $\Sigma(\infty)$. [One can also understand these two cases in terms of Fig. 4: as the number of tensile cycles increase, the pair of nucleation lines associated with the transitions $A \leftrightarrow M^+$ translate to the right. In particular, the point at which the $M^+ \to A$ nucleation line in Fig. 4(c) intersects the temperature axis also moves to the right and eventually settles at a certain location when $n \to \infty$. The condition on θ stated above which distinguishes these two cases is precisely that for which the point $(\theta, 0)$ lies to the left or the right of this limiting point.]

Figure 5(b) shows the analogous stress–elongation loops during compressive loading cycles. In this case the hysteresis loop shifts upwards with increasing load cycles.

(ii) Figure 6 shows the stress–elongation response of an austenitic bar that is subjected to a cyclic extension whose amplitude increases progressively. Experimental observations in such a test, resulting in a similar staircase response, have been reported by Kyriakides and Shaw (1995). The amplitude is moderately large; large enough to nucleate the $A \to M^+$ transition but not so large as to carry out the transformation to completion. Thus, in each cycle the specimen transforms from austenite to martensite over some length of the bar and the extent of the bar that undergoes this transition increases from one cycle to the next. During the first cycle, a phase boundary nucleates at the left end of the bar, propagates some distance L_1 ($<L$) along the bar and then retracts back to the left end. In the second cycle, the phase boundary propagates a greater distance L_2 along the bar ($L_1 < L_2 < L$)

before reversing its direction, etc. Figure 6 shows the response of this bar as calculated from our model. The hysteresis loop shows a "staircase" effect due to the fact that different pieces of the bar have undergone different transformation histories.

Consider, for example the loading portion of the third cycle. In view of its past history, the segment $(0, L_1)$ has previously undergone the $A \to M^+$ transformation twice, and therefore, for these particles $\overset{+}{n} = 2$; the adjacent segment (L_1, L_2) has undergone this transformation once previously, and so here $\overset{+}{n} = 1$; the rest of the bar (L_2, L) has never undergone the austenite–martensite transformation and so here $\overset{+}{n} = 0$. Thus, by eqns (16a) and (17), the stress level during the loading portion of the third cycle is

$$\sigma = \sigma_{cr} + \sigma_0(\theta) - \Sigma(3) \tag{23}$$

when the phase boundary is propagating through the segment $(0, L_1)$ of the bar; it is

$$\sigma = \sigma_{cr} + \sigma_0(\theta) - \Sigma(2) \tag{24}$$

when the phase boundary is propagating through the next segment (L_1, L_2) of the bar; and is given by

$$\sigma = \sigma_{cr} + \sigma_0(\theta) - \Sigma(1) \tag{25}$$

when it is propagating through the rest of the bar. The values of L_1 and L_2 are known (they are determined by the amounts of elongation in the first two cycles). In order to complete the description of this loading process, one merely needs to note from eqn (20) that when the phase boundary is at some general location $x = s$, the elongation is given by

$$\delta = [\sigma/\mu + \alpha(\theta - \theta_T)]L + \gamma_T s. \tag{26}$$

Figure 6 may now be constructed, for the loading stage of the third cycle, as follows: (a) the entire bar first consists of austenite and eqn (26) holds with $s = 0$. This is valid for values of stress less than that given by eqn (23). (b) During the second stage we have $0 < s < L_1$ in eqn (26) and the stress remains constant at the value give by eqn (23). (c) During the next stage we have $s = L_1$ (eqn 26) and the stress increases from the value given in eqn (23) to that in eqn (24). (d) In the fourth stage we have $L_1 < s < L_2$ in eqn (26) and the stress remains at the value given by eqn (24). (e) In the fifth stage, $s = L_2$ in eqn (26) and the stress increases from the value given in eqn (24) to that in eqn (25), etc.

(iii) We now turn to a different simulation. Consider cyclic mechanical loading at a fixed temperature θ, similar to that discussed at the beginning of this section, but now with a loading amplitude which varies from compression to tension. We first discuss the response heuristically. The stress–elongation response, at least for sufficiently high temperatures, will consist of a combination of the tensile and compressive hysteresis loops shown in Fig. 5(a, b), leading to a response similar to that shown in Fig. 7(a). As the number of load cycles increase, the upper hysteresis loop drifts downwards and the lower loop drifts upwards (recall discussion pertaining to Fig. 5). Thus, in particular, the vertical separation between the two lower plateaus of the two hysteresis loops decreases as the number of cycles increases and likewise, so does the distance between the two upper plateaus. Eventually, under suitable conditions, these plateaus will coincide and the response will look like that shown in Fig. 7(b), where the transformation is now between the two variants of martensite, and does not involve austenite. From hereon there is no $A \to M^{\pm}$ transformation, and so the internal variables $\overset{\pm}{n}$ do not change their values and thus the response no longer changes.

We now consider this more carefully. The loading path in the θ, σ-plane of Fig. 4 is a vertical line through $(\theta, 0)$ with its two end points in the M^- and M^+ regions. Suppose that $\theta > \theta_T[1 + \sigma_{cr}\gamma_T/(2\rho\lambda_T)]$; the right hand side of this inequality denotes the temperature associated with the point at which the $M^- \to A$ and $M^- \to M^+$ nucleation lines intersect in Fig. 4(a). Then, at least in the first cycle, Fig. 4(a) implies that the bar goes from M^- to A

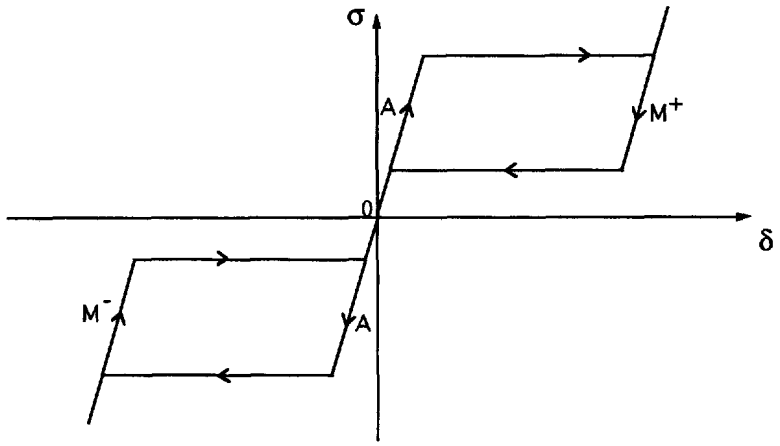

(a) Response in first cycle

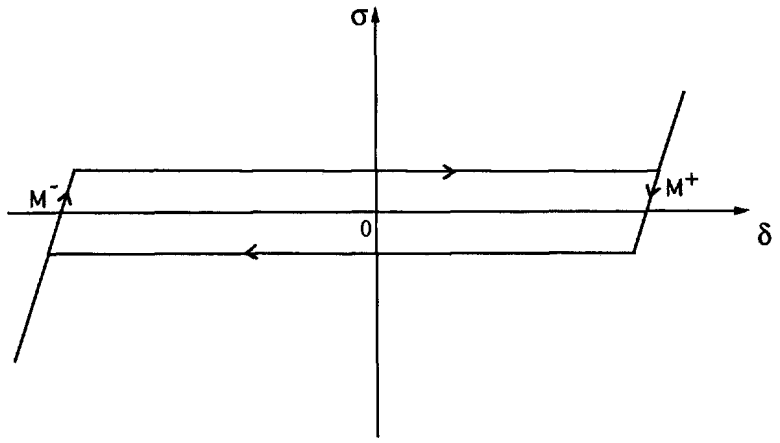

(b) Response after a number of cycles

Fig. 7. Cyclic loading involving tensile and compressive stress.

to M^+ during loading and from M^+ to A to M^- on unloading. Figure 7(a) shows the corresponding stress–elongation hysteresis loops; the tensile loop is described by eqns (19)–(22) with $n = 1$, with similar formulas describing the compressive loop. At the end of each complete loading–unloading cycle, one has $\overset{+}{n} = \bar{n}$ and this (common value) increases with each cycle. Thus, the nucleation lines in Fig. 4 progressively translate to the right and in particular, so does the point of intersection of the $M^- \to A$ and $M^- \to M^+$ nucleation lines. The nucleation diagram for subsequent cycles is the one shown in Fig. 4(b). If $\theta/\theta_T < 1 + \sigma_{cr}\gamma_T/(2\rho\lambda_T) + \gamma_T\Sigma(\infty)/(\rho\lambda_T)$, then after N cycles, the point at which the $M^- \to A$ and $M^- \to M^+$ nucleation lines intersect will reach the vertical line $\theta =$ constant. When this happens, the loading path $\theta =$ constant no longer encounters the austenitic region, and so the bar transforms directly between M^+ and M^-. The number of cycles N at which this happens is given by the root of the equation $\theta/\theta_T = 1 + \sigma_{cr}\gamma_T/(2\rho\lambda_T) + \gamma_T\Sigma(N)/(\rho\lambda_T)$. Figure 7(b) shows the stress–elongation hysteresis loop for $n \geqslant N$. The stress plateaus here are given by eqn (16) with $n = N$. As noted previously, since the austenite–martensite transitions have ceased to occur, the values of $\overset{+}{n}$ and $\bar{n}$ do not change further, and the nucleation diagram and the associated stress–elongation hysteresis loop do not alter with continued cycling for $n \geqslant N$.

It is interesting to note that in Au–Cd shape-memory alloys, Lieberman *et al.* (1975) have observed that the stress–elongation hysteresis behavior changes from that shown in Fig. 7(a) to that shown in Fig. 7(b) after cycling through many cycles. The reason underlying this phenomenon is the so-called "shift-relaxation" microscopic mechanism which has recently been analyzed by Bhattacharya *et al.* (1996).

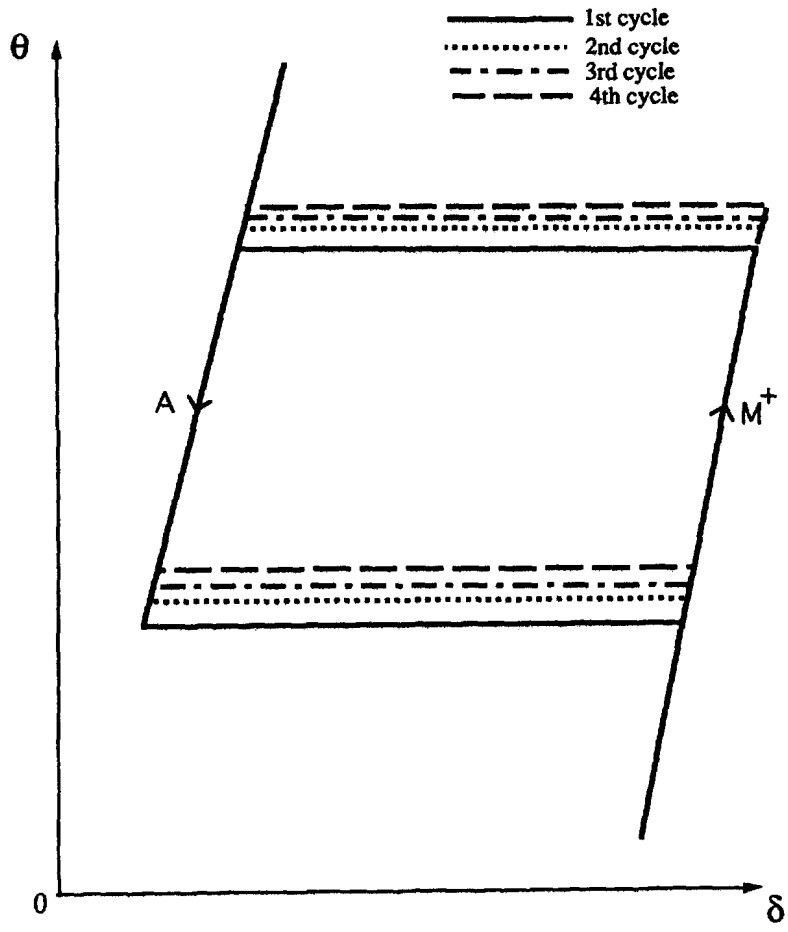

Fig. 8. Thermal loading under constant tensile stress: temperature–elongation loops.

(iv) We turn next to thermal cycling at, say, a constant tensile stress σ. The loading path in Fig. 4 is now a segment of the horizontal line σ = constant. According to our model, the response of the specimen in the nth -cycle is characterized as follows: from eqn (2a), when the bar consists entirely of austenite

$$\theta = \frac{\delta}{\alpha L} - \frac{\sigma}{\mu\alpha} + \theta_T; \tag{27}$$

by eqns (7a), (11), (16a) and (17), the transformation from $A \to M^+$ occurs at the constant temperature.

$$\theta = M_s + \frac{\gamma_T \theta_T}{\rho \lambda_T}[\sigma + \Sigma(n)]; \tag{28}$$

by eqn (2b), when the bar consists entirely of martensite one has

$$\theta = \frac{\delta}{\alpha L} - \frac{\gamma_T}{\alpha} - \frac{\sigma}{\mu\alpha} + \theta_T; \tag{29}$$

and by eqns (7b), (11), (16a) and (17), the reverse transformation from $M^+ \to A$ occurs at

$$\theta = A_s + \frac{\gamma_T \theta_T}{\rho \lambda_T}[\sigma + \Sigma(n)], \tag{30}$$

where A_s and M_s were defined in eqn (11). Figure 8 shows the temperature–elongation

hysteresis loops for the first four cycles of such a loading program. Equations (28) and (30) describe the lower and upper plateaus of the hysteresis loop. The loop drifts upwards as n increases. A response similar to this has been observed in experiments, (Tobushi *et al.*, 1991).

(v). Finally we consider the two-way shape-memory effect using our constitutive model. Consider a virgin specimen of austenite and suppose that it is subjected to thermal cycling at zero stress. From Fig. 4(a), the description of nucleation sites at the beginning of this section, and the kinetic relation (17), we conclude that, in the first cycle, the phases M^+ and M^- are nucleated simultaneously at the two ends of the bar when $\theta = M_s$; the two resulting phase boundaries then move with equal speed towards the midpoint of the bar. Since the transformation strain of M^+ is $+\gamma_T$ and that of M^- is $-\gamma_T$, and since at all instants the bar consists of equal amounts of M^+ and M^-, the bar does not change length due to transformation. In subsequent cycles, one always has $\overset{+}{n} = \overset{-}{n}$ and, therefore, from Fig. 4(b) we see that the scenario of the first cycle continues to be true. Thus, the only length change during thermal cycling at zero stress is small and due to the coefficient of thermal expansion; a graph of elongation versus temperature is a straight-line of slope $1/(\sigma L)$.

Suppose now, that before subjecting the above bar to thermal cycling, it was first subjected to mechanical tensile cycling at a constant (and suitable value of) temperature. The $A \leftrightarrow M^+$ transformation that occurs during the mechanical cycling increases the value of $\overset{+}{n}$ while $\overset{-}{n}$ remains zero. After such mechanical cycling ("training") the relevant nucleation diagram is Fig. 4(c). If the bar is now subjected to thermal cycling at zero stress, we see from this figure that the transformation that occurs is $A \leftrightarrow M^+$ (rather than $A \leftrightarrow$ a mixture of M^+ and M^- as it was before training). Therefore, the bar elongates appreciably upon cooling due to the positive transformation strain $+\gamma_T$ associated with the formation of M^+; when the bar is heated, it shortens as M^+ goes back to austenite. The response is now similar to that shown in Fig. 8.

Note from Fig. 4 that, according to our model, there are other ways in which to "train" a bar in order to induce the two-way shape-memory effect, e.g. by going through thermal cycling at a constant tensile stress, or by subjecting it to the one-way shape-memory effect many times; in each of these cases the training causes $\overset{+}{n}$ to increase with no change in $\overset{-}{n}$.

Acknowledgements—Useful discussions with Stelios Kyriakides and John Shaw (University of Texas at Austin), and Dimitri Lagoudas and Jay Walton (Texas A & M) are gratefully acknowledged. This work was supported by the National Science Foundation and the Office of Naval Research.

REFERENCES

Abeyaratne, R., Kim, S.-J. and Knowles, J. K. (1994). A one-dimensional continuum model for shape-memory alloys. *International Journal of Solids and Structures* **31**, 2229–2249.

Abeyaratne, R. and Knowles, J. K. (1993). A continuum model of a thermoelastic solid capable of undergoing phase transitions. *Journal of the Mechanics and Physics of Solids* **41**, 541–571.

Bhattacharya, K., James, R. D. and Swart, P. (1996). Relaxation in shape memory alloys. *Acta Materzlia* (submitted).

Brinson, L. C. and Lammering, R. (1993). Finite element analysis of the behavior of shape memory alloys and their applications. *International Journal of Solids and Structures* **30**, 3261–3280.

Falk, F. Model free energy, mechanics and thermodynamics of shape memory alloys. *Acta Metallurgica* **28**, 1773–1780.

Graesser, E. J. and Cozzarelli, F. A. (1994). A proposed three-dimensional constitutive model for shape memory alloys. *Journal of Intelligent Materials Systems and Structures* **5**, 78–89.

Kawaguchi, M., Ohashi, Y. and Tobushi, H. (1991). Cyclic characteristics of pseudoelasticity of Ti-Ni alloys. *JSME International Journal* **34**, 76–82.

Kim, S.-J. and Abeyaratne, R. (1995). Cyclic effects in shape-memory alloys: a simple continuum model. Caltech ONR Technical Report No. 6, June.

Kyriakides, S. and Shaw, J. A. (1993). Work in progress. For preliminary results see Kyriakides, S., Shaw, J. A. and Abeyaratne, R. Material characterization of shape memory alloys, EMRL Report No. 93/6, The University of Texas, Austin.

Lieberman, D. S., Schmerling, M. A. and Karz, R. S. (1975). Ferroelastic memory and mechanical properties in Gold-Cadmium. In *Shape Memory Effect in Alloys* (Edited by J. Perkins), pp. 203–242. Plenum Press.

Lin, P. H., Tobushi, H., Tanaka, K., Hattori, T. and Makita, M. (1994). Pseudoelastic behavior of TiNi shape memory alloy subjected to strain variations. *Journal of Intelligent Materials Systems and Structures* **7**, 399–410.

Melton, K. N. and Mercier, O. (1979). Fatigue of NiTi thermoelastic martensites. *Acta Metallurgica* **27,** 137–144.

Miyazaki, S., Imai, T., Igo, Y. and Otsuka, K. (1986a). Effect of cyclic deformation on the pseudoelasticity characteristics of Ti-Ni alloys. *Metallurgy Transactions* **17A,** 115–120.

Miyazaki, S., Igo, Y. and Otsuka, K. (1986b). Effect of thermal cycling on the transformation temperatures of Ti-Ni alloys. *Acta Metallurgica* **34,** 2045–2051.

Müller, I. and Wilmansky, K. (1981). Memory alloys—phenomenology and Ersatzmodel. In *Continuum Models of Discrete Systems* (Edited by O. Brulin and R. K. T. Hsieh), pp. 495–509. North Holland, Amsterdam.

Müller, I. and Xu, H. (1991). On the pseudoelastic hysteresis. *Acta Metallurgica Materials* **39,** 263–271.

Ortin, J. (1992). Preisach modeling of hysteresis for a pseudoelastic CuZnAl single crystal. *Journal of Applied Physics* **71,** 1454–1461.

Perkins, J. and Sponholz, R. O. (1984). Stress-induced martensitic transformation cycling and two-way shape memory training in Cu–Zn–Al alloys. *Metallurgy Transactions* **15A,** 313–321.

Raniecki, B., Lexcellent, C. and Tanaka, K. (1992). Thermodynamic models of pseudoelastic behavior of shape memory alloys. *Archives of Mechanics* **44,** 261–288.

Tanaka, K., Hayashi, T., Itoh, Y. and Tobushi, H. (1992). Analysis of thermomechanical behavior of shape memory alloys. *Mechanics and Materials* **13,** 207–215.

Tanaka, K., Hayashi, T. and Itoh, Y. (1993). Phenomenological analysis on subloops and cyclic behavior in shape memory alloys under mechanical and/or thermal loads. Preprint.

Tobushi, H., Iwanaga, H., Tanaka, K., Hori, T. and Sawada, T. (1991). Deformation behavior of TiNi shape memory alloy subjected to variable stress and temperature. *Continuous Mechanical Thermodynamics* **3,** 79–93.